Acta Mechanica 84, 89—107 (1990)

ACTA MECHANICA

Dynamic shear band development in plane strain compression of a viscoplastic body containing a rigid inclusion

Z. G. Zhu and **R. C. Batra**, Rolla, Missouri

(Received October 18, 1989; revised January 3, 1990)

Summary. We study the plane strain thermomechanical deformations of a viscoplastic body containing a rigid non-heat-conducting ellipsoidal inclusion at the center. Two different problems, one in which the major axis of the inclusion is parallel to the axis of compression and the other in which it is perpendicular to the loading axis are considered. In each case the deformations are presumed to be symmetric about the two centroidal axes and consequently deformations of a quarter of the block are analyzed. The material of the block is assumed to exhibit strain-rate hardening, but thermal softening. The applied load is such as to cause deformations of the block at an overall strain-rate of 5000 sec^{-1}. The rigid inclusion simulates the presence of second phase particles such as oxides or carbides in a steel and acts as a nucleus for the shear band.

It is found that a shear band initiates near the tip of the inclusion and propagates along a line inclined at 45° to the horizontal axis. At a nominal strain of 0.25, the peak temperature rise near the tip of the vertically aligned inclusion equals 75% of that for the horizontally placed inclusion. The precipitous drop in the effective stress near the inclusion tip is followed somewhat later by a rapid rise in the maximum principal logarithmic strain there.

1 Introduction

A phenomenon which is commonly observed during high strain rate inelastic deformation of metals is the formation of narrow bands of intense shear strain usually called adiabatic shear bands. These shear bands form during high speed material processing, metal forming, and ballistic penetration. This is an important mode of deformation as these shear zones often become the sites for eventual failure of the material.

Since the time Zener and Hollomon [1] recognized the destabilizing effect of thermal softening in reducing the slope of the stress-strain curve in nearly adiabatic deformations, there have been many analytical (e.g. Recht [2], Staker [3], Clifton [4], Clifton and Molinari [5], Burns [6], Wright [7], Anand et al. [8], Bai [9], Coleman and Hodgdon [10]), experimental (e.g. Moss [11], Costin et al. [12], Marchand and Duffy [13]) and numerical (e.g. Clifton et al. [14], Merzer [15], Wu and Freund [16], Wright and Batra [17], [18], Wright and Walter [19], Batra [20]—[22], LeMonds and Needleman [23], [24], Needleman [25], Batra and Liu [26], [27], Anand et al. [28]) studies aimed at understanding the factors that enhance or inhibit the shear strain localization.

Although it is well recognized that dynamic fracture is significantly influenced by grain boundaries, precipitates and inclusions, inherent voids and flaws, texture, substructure, and impurities [29], very little is known about how such microstructural features influence shear band nucleation and growth. Most computational shear band models are

based on the relative ability of a material to work harden and thermal soften, and metallurgical influences are taken into account only implicitly as they influence the stress-strain and strength-temperature curves. The presence of a material defect has usually been modeled by introducing either a temperature perturbation [19]—[22], [26]—28] or assuming that the material at the site of the defect is weaker than the surrounding material [25], [27]. Of the numerical studies cited above, LeMonds and Needleman [23], [24], Needleman [25], Batra and Liu [26], [27] and Anand et al. [28] have analyzed the development of a shear band in plane strain problems. Of these, only Needleman and Batra and Liu have considered the effect of inertia forces. Whereas Batra and Liu assumed that the material softens because of its being heated up, Needleman studied a mechanical problem and accounted for softening mechanisms through the use of an internal variable.

In this paper, we study the thermomechanical plane strain deformations of a thermally softening viscoplastic solid and model the material inhomogeneity by introducing a rigid perfectly insulated cylindrical inclusion at the center of the block. The inclusion can be viewed as precipitates or second phase particles in an alloy. These particles, such as oxides or cairbides, are usually very strong relative to the surrounding material, and their deformat ons can be neglected. Here we also take the inclusion to be non-heat conducting. Whereas Batra and Liu [26], [27] modeled the thermal softening of the material by a linear relation, we assume that the flow stress decreases exponentially with a rise in temperature. Thus, the material never looses its strength entirely even though it becomes quite small at very high temperatures. The problem formulation incorporates the effect of inertia forces, strain-rate sensitivity and heat conduction. The coupled nonlinear equations expressing the balance of mass, linear momentum and internal energy are solved numerically for a prescribed set of initial and boundary conditions.

2 Formulation of the problem

We study plane strain thermomechanical deformations of a cylindrical body having a square cross-section and presume that there is a rigid inclusion whose centroidal axis coincides with that of the body. The cross-section of the inclusion is taken to be elliptical with the major axis either parallel to or perpendicular to the axis of loading.

We use an updated Lagrangian description [30], where in order to solve for the deformations of the body at time $(t + \Delta t)$, the configuration at time t is taken as the reference configuration. However, the deformations of the body from time t to time $(t + \Delta t)$ could be finite. With respect to a fixed set of rectangular Cartesian coordinates axes, we denote the position of a material particle in the configuration at time t by X_α and in the configuration at time $(t + \Delta t)$ by x_i. In terms of the referential description, the governing equations for the deformable matrix can be written as

$$(\varrho J)^{\cdot} = 0, \tag{2.1}$$

$$\varrho_0 \dot{v}_i = T_{i\alpha,\alpha}, \tag{2.2}$$

$$\varrho_0 \dot{e} = -Q_{\alpha,\alpha} + T_{i\alpha} v_{i,\alpha}, \tag{2.3}$$

which ought to be supplemented by appropriate constitutive relations, and initial and boundary conditions. Equations (2.1), (2.2), and (2.3) express, respectively, the balance of mass, the balance of linear momentum, and the balance of internal energy. Here ϱ is the

mass density of a material particle in the current configuration at time $t + \Delta t$, ϱ_0 its mass density in the reference configuration at time t, a superimposed dot expresses a material time derivative, $J = \varrho_0/\varrho$ equals the determinant of the deformation gradient $F_{i\alpha} = x_{i,\alpha}$, v_i is the velocity of a material particle in the x_i-direction, $T_{i\alpha}$ is the first Piola-Kirchhoff stress tensor, a comma followed by $\alpha(i)$ implies partial differentiation with respect to $X_\alpha(x_i)$, the usua summation convention over repeated indices has been used, e is the specific internal energy, and Q_α is the heat flux measured per unit area in the reference configuration. In plane strain deformations in the $x_1 - x_2$ plane, the subscripts α and i range over 1 and 2.

The following constitutive equations are employed to describe the matrix response:

$$\sigma_{ij} = -p(\varrho)\,\delta_{ij} + 2\mu D_{ij}, \tag{2.4}$$

$$T_{i\alpha} \equiv (\varrho_0/\varrho)\,X_{\alpha,j}\sigma_{ij}, \tag{2.5}$$

$$2\mu = \left[\sigma_0/\left(\sqrt{3}\,I\right)\right] e^{-\nu\theta}(1 + bI)^m, \tag{2.6}$$

$$Q_\alpha = -(\varrho_0/\varrho)\,kX_{\alpha,j}\theta_{,j}, \tag{2.7}$$

$$2D_{ij} = v_{i,j} + v_{j,i}, \tag{2.8}$$

$$2I^2 = \tilde{D}_{ij}\tilde{D}_{ij}, \qquad \tilde{D}_{ij} = D_{ij} - \frac{1}{3}\,D_{kk}\delta_{ij}, \tag{2.9}$$

$$p(\varrho) = B(\varrho/\varrho_r - 1), \tag{2.10}$$

$$\varrho_0\dot{e} = \varrho_0 c\dot{\theta} + \varrho_0\dot{\varrho}p(\varrho)/\varrho^2, \tag{2.11}$$

where σ_{ij} is the Cauchy stress tensor, σ_0 is the stress in a quasi-static simple tension or compression test, ν is the coefficient of thermal softening, $\tilde{D}_{ij}$ is the deviatoric strain rate tensor, D_{ij} is the strain-rate tensor, δ_{ij} is the Kronecker delta, B may be interpreted as the bulk modulus, ϱ_r is the mass density in the stress free reference configuration, c is the specific heat, k the thermal conductivity, and parameters b and m describe the strain-rate sensitivity of the material. Here ν, σ_0, k, c, b and m are taken to be independent of the temperature. Equation (2.7) is the Fourier law of heat conduction, referred to the reference configuration.

Introducing non-dimensional variables

$$\begin{aligned}
&\bar{\boldsymbol{\sigma}} = \boldsymbol{\sigma}/\sigma_0, && \bar{p} = p/\sigma_0, && \bar{\mathbf{s}} = \mathbf{s}/\sigma_0, && \bar{\boldsymbol{v}} = \boldsymbol{v}/v_0, && \\
&\bar{t} = tv_0/H, && \bar{\boldsymbol{T}} = \boldsymbol{T}/\sigma_0, && \bar{\boldsymbol{x}} = \boldsymbol{x}/H, && \bar{\theta} = \theta/\theta_0, && \\
&\bar{b} = bv_0/H, && \bar{\nu} = \nu\theta_0, && \bar{\varrho} = \varrho/\varrho_r, && \bar{\varrho} = \varrho_0/\varrho_r, && \bar{\boldsymbol{X}} = \boldsymbol{X}/H, \\
&\delta = \varrho_r v_0^2/\sigma_0, && \beta = k/(\varrho_r c v_0 H), && \theta_0 = \sigma_0/(\varrho_r c), && \bar{B} = B/\sigma_0, &&
\end{aligned} \tag{2.12}$$

the governing equations become

$$\dot{\varrho} + \varrho v_{i,i} = 0, \tag{2.13}$$

$$\delta\tilde{\varrho}\dot{v}_i = T_{i\alpha,\alpha}, \tag{2.14}$$

$$\tilde{\varrho}\dot{\theta} = -Q_{\alpha,\alpha} + (\tilde{\varrho}/\varrho)\left[1/\left(\sqrt{3}\,I\right)\right](1 + bI)^m\, e^{-\nu\theta}\tilde{D}_{ij}\tilde{D}_{ij}, \tag{2.15}$$

$$Q_\alpha = -\frac{\tilde{\varrho}}{\varrho}\,\beta X_{\alpha,j}\theta_{,j}, \tag{2.16}$$

$$\sigma_{ij} = -B(\varrho - 1)\,\delta_{ij} + \left[1/\left(\sqrt{3}\,I\right)\right](1 + bI)^m\, e^{-\nu\theta}D_{ij}, \tag{2.17}$$

where the superimposed bars have been dropped. In Eq. (2.12), $2H$ is the height of the block and v_0 the imposed velocity on the top and bottom surfaces. In Eqs. (2.13)—(2.17) all of the differentiations are with respect to non-dimensional variables.

For the simple compression problem, we restrict ourselves to deformations that remain symmetrical about both $X_1 = 0$ and $X_2 = 0$. With the nondeformable and non-heat-conducting inclusion, the boundary conditions for the material in the first quadrant are:

$$\begin{aligned}
&v_1 = 0, \quad T_{21} = 0, \quad Q_1 = 0 && \text{at } x_1 = X_1 = 0,\\
&v_2 = 0, \quad T_{12} = 0, \quad Q_2 = 0 && \text{at } x_2 = X_2 = 0,\\
&T_{i\alpha}N_\alpha = 0, \quad Q_\alpha N_\alpha = 0 && \text{on the right surface,}\\
&v_2 = -U(t), \quad T_{12} = 0, \quad Q_2 = 0 && \text{on the top face,}\\
&v_1 = 0, \quad v_2 = 0, \quad Q_\alpha N_\alpha = 0 && \text{at the interface } \Gamma_0 \text{ between the inclusion and the matrix.}
\end{aligned} \tag{2.18}$$

That is, boundary conditions resulting from the assumed symmetry of deformations are applied on the left and bottom faces, the right face of the block is taken to be traction free, and a prescribed normal velocity and zero tangential tractions are applied on the top face. All four sides of the block are assumed to be perfectly insulated. The zero velocity and the zero heat flux at interface Γ_0 implies that the second phase particle is rigid and non-heat-conducting.

The interface Γ_0 between the inclusion and the matrix has the parametric representation

$$\frac{X_1^2}{a^2} + \frac{X_2^2}{b^2} = 1 \quad \text{or} \quad \frac{x_1^2}{a^2} + \frac{x_2^2}{b^2} = 1, \tag{2.19}$$

where $2a$ and $2b$ are the major and minor axes of the ellipse respectively.

For the initial conditions we take

$$\varrho(\boldsymbol{X}, 0) = 1.0, \quad v_1(\boldsymbol{X}, 0) = 0, \quad v_2(\boldsymbol{X}, 0) = 0, \quad \theta(\boldsymbol{X}, 0) = 0, \tag{2.20}$$

and the loading path is

$$U(t) = \begin{cases} t/0.005 & 0 \leqq t \leqq 0.005, \\ 1 & t \geqq 0.005. \end{cases} \tag{2.21}$$

3 Finite element formulation of the problem

Because of our inability to solve the coupled nonlinear partial differential equations (2.13) to (2.16) analytically, we seek an approximate numerical solution of the problem by the finite element method. By using the Galerkin method and the lumped mass matrix (e.g. see Hughes [31]), we obtain the following semi-discrete formulation of the problem from Eqs. (2.13) — (2.16), boundary conditions (2.18), and initial conditions (2.20).

$$\dot{\boldsymbol{d}} = \boldsymbol{F}(\boldsymbol{d}, \delta, \beta, b, m, \nu), \tag{3.1}$$

$$\boldsymbol{d}(o) = \boldsymbol{d}_0. \tag{3.2}$$

Here $\boldsymbol{d}$ is the vector of nodal values of the mass density, two components of the velocity and the temperature. The number of nonlinear ordinary differential equations (3.1) equals

four times the number of nodes. These differential equations are solved by using the backward difference Adams method included in the IMSL subroutine LSODE. The subroutine adjusts the time increment adaptively until it can compute a solution of (3.1) and (3.2) to the prescribed accuracy.

Batra and Liu [26], [27] initially used 9-noded quadrilateral elements. Their subsequent work [32] revealed that 4-noded quadrilateral elements provide a better resolution of the intense deformation within the region of localization. Thus, we use here 4-noded quadrilateral elements. The finite element code developed by Batra and Liu [26] was modified to include the exponential thermal softening of the material.

4 Numerical results

The following values of material and geometric parameters used in the calculations are representative of a typical hard steel.

$$
\begin{aligned}
&b = 10{,}000\ \text{sec}, \quad \sigma_0 = 333\ \text{MPa}, \quad k = 49.22\ \text{Wm}^{-1}\,^{\circ}\text{C}^{-1}, \quad m = 0.025,\\
&c = 473\ \text{J Kg}^{-1}\,^{\circ}\text{C}^{-1}, \quad \varrho_r = 7{,}860\ \text{Kg m}^{-3}, \quad B = 128\ \text{GPa},\\
&H = 5\ \text{mm}, \quad v_0 = 25\ \text{msec}^{-1}, \quad \nu = 0.0025\,^{\circ}\text{C}^{-1},\\
&a = 0.2, \quad b = 0.02 \quad \textit{or} \quad a = 0.02 \quad \text{and} \quad b = 0.2.
\end{aligned}
\tag{4.1}
$$

FINITE ELEMENT MESH FOR SHEAR BAND

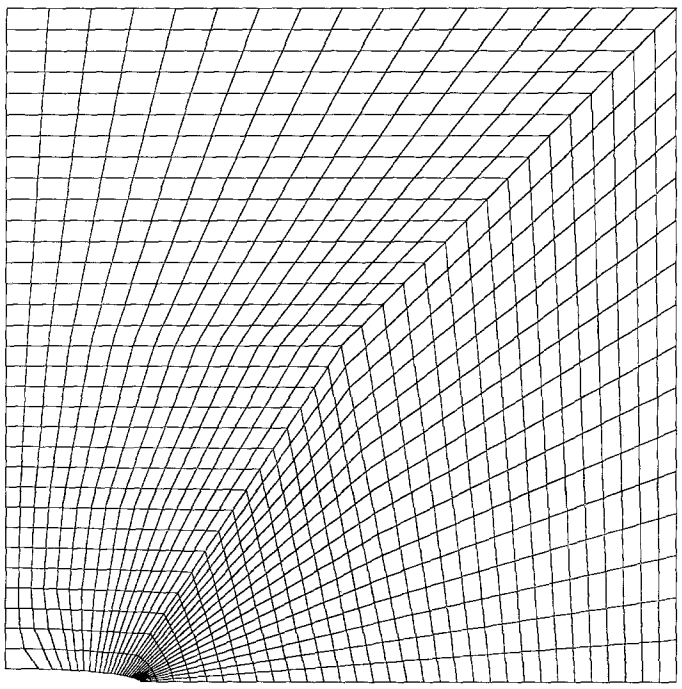

Fig. 1. The finite element mesh used for the analysis of the problem when the rigid elliptic inclusion is placed horizontally

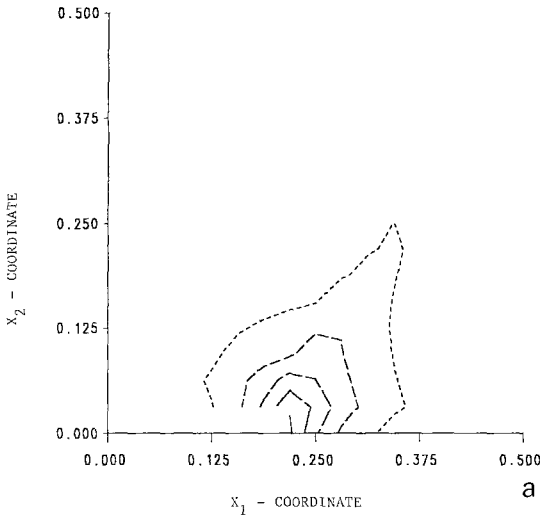
0.500
0.375
0.250
0.125
0.000
X_2 - COORDINATE
0.000 0.125 0.250 0.375 0.500
X_1 - COORDINATE
a

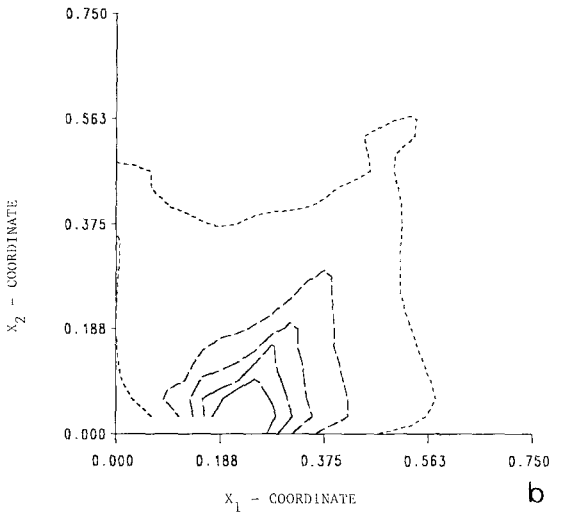
0.750
0.563
0.375
0.188
0.000
X_2 - COORDINATE
0.000 0.188 0.375 0.563 0.750
X_1 - COORDINATE
b

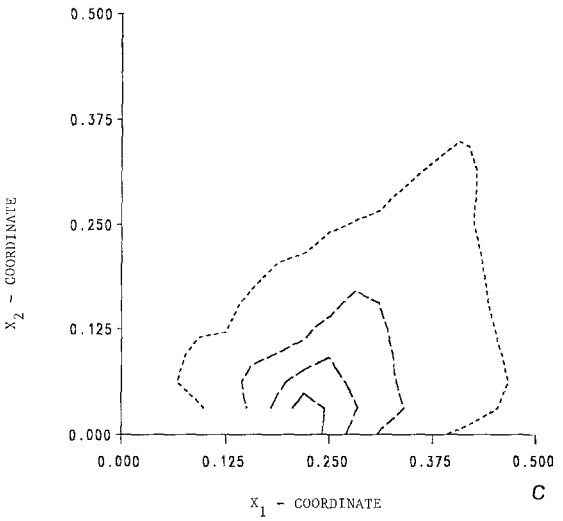
0.500
0.375
0.250
0.125
0.000
X_2 - COORDINATE
0.000 0.125 0.250 0.375 0.500
X_1 - COORDINATE
c

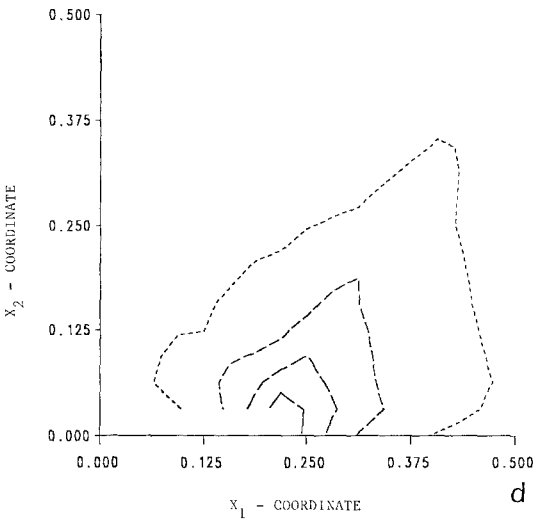
0.500
0.375
0.250
0.125
0.000
X_2 - COORDINATE
0.000 0.125 0.250 0.375 0.500
X_1 - COORDINATE
d

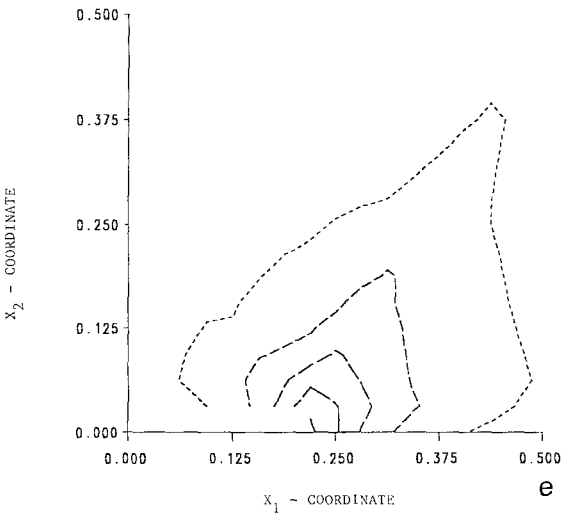
0.500
0.375
0.250
0.125
0.000
X_2 - COORDINATE
0.000 0.125 0.250 0.375 0.500
X_1 - COORDINATE
e

For values given in (4.1), $\theta_0 = 89.6\,^{\circ}\mathrm{C}$ and the average applied strain-rate equals $5000\ \mathrm{sec}^{-1}$. Figure 1 depicts the finite element mesh used in the computations when the major axis of the elliptic inclusion is along the x_1-axis. The aspect ratio of the elliptical inclusion is taken to be large so as to increase the stress concentration near the vertex of the major axis and reduce the CPU time required to solve the problem. The finite element mesh used is very fine in the region surrounding the edge of the inclusion and gradually becomes coarser as we move away from it. A similar mesh is used when the major axis of the inclusion is vertical. We note that we have not made any attempt to align the element sides along the direction of maximum shearing. Needleman [25] has used a mesh with the element sides aligned along the expected direction of development of the shear band.

The isotherms at five different values of the average strain are plotted in Figs. 2a through 2e for the horizontally placed elliptic inclusion, and Figs. 3a through 3e for the vertically oriented elliptic inclusion. Due to the high stress concentration at the tip of the inclusion, the material near the tip is severely deformed and gets heated up faster than the rest of the block. The built up heat makes the material softer but the softer material cannot deform very rapidly because of the constraints imposed on it by the surrounding material. Also the heat slowly conducts out of this relatively warmer region. With continued further straining of the block, the material near the inclusion tip becomes sufficiently hot that thermal softening effect exceeds the hardening due to the straining of the material. Even though the material point near the inclusion tip may become unstable, a shear band need not initiate at this time. For example, the one-dimensional numerical studies [19]—[22] make it clear that a shear band usually initiates at a value of nominal strain far in excess of the value at which the shear stress attains its peak value. Once a shear band initiates, the material within the band gets heated up very fast. As the shear band grows, the rate of temperature rise at the inclusion tip slows down. We have plotted in Figs. 4a and 4b the temperature rise at six points within the deforming region as a function of the average strain for each of the two cases considered. In each case, the temperature rises at a point near the inclusion tip much faster than that at points away from it. The rate of temperature rise at points near the inclusion tip decreases gradually and eventually attains a constant value. At points far removed from the inclusion tip, the rate of temperature increase is essentially uniform implying thereby that the small regions surrounding these points are deforming homogeneously. Even though the results for the horizontally and vertically aligned inclusions are similar in nature the temperature rise near the inclusion tip for the vertically aligned inclusion is considerably less as compared to that for the horizontally placed inclusion. In each case, the contours of constant temperature propagate along lines inclined at 45° to the horizontal axis. In the absence of an inclusion, this will be the direction of the maximum shearing stress.

The variation of the effective stress s_e defined by

$$s_e^2 = \frac{1}{2} S_{ij} S_{ij}, \qquad S_{ij} = \sigma_{ij} + \left(p - \frac{2}{3}\mu D_{kk}\right)\delta_{ij}, \tag{4.2}$$

Fig. 2. Isotherms plotted in the reference configuration at different values of the average strain with the horizontally placed inclusion

(a) $\gamma_{avg} = 0.0536$, $\theta_{max} = 5.17$ ---- 1; - - - - 2; — — — — 3; ——— 4; ——— 5.
(b) $\gamma_{avg} = 0.1486$, $\theta_{max} = 8.63$. See part (a) for values of θ corresponding to different curves.
(c) $\gamma_{avg} = 0.1887$, $\theta_{max} = 9.62$. ---- 2; - - - - 4; — — — — 6; ——— 8; ——— 10.
(d) $\gamma_{avg} = 0.2008$, $\theta_{mag} = 9.82$. See part (c) for values of θ corresponding to different curves.
(e) $\gamma_{avg} = 0.2478$, $\theta_{max} = 10.46$. See part (c) for values of θ corresponding to different curves

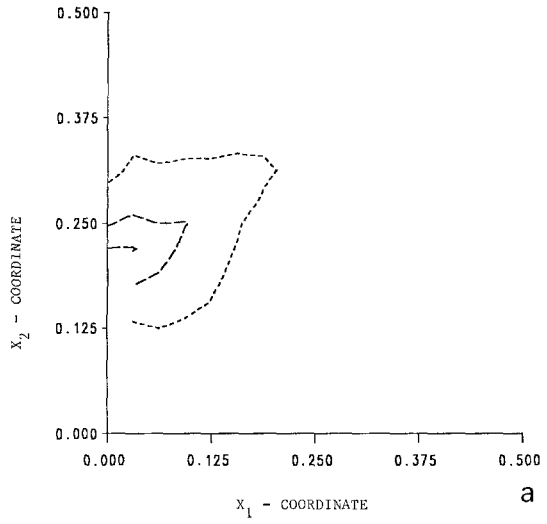
0.500
0.375
0.250
0.125
0.000
0.000
0.125
0.250
0.375
0.500
X_2 - COORDINATE
X_1 - COORDINATE
a

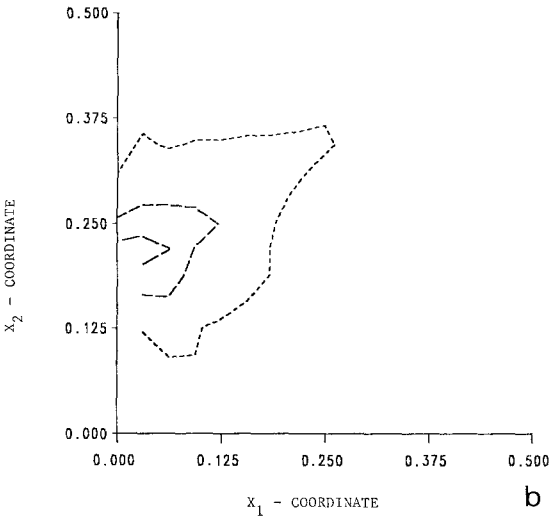
0.500
0.375
0.250
0.125
0.000
0.000
0.125
0.250
0.375
0.500
X_2 - COORDINATE
X_1 - COORDINATE
b

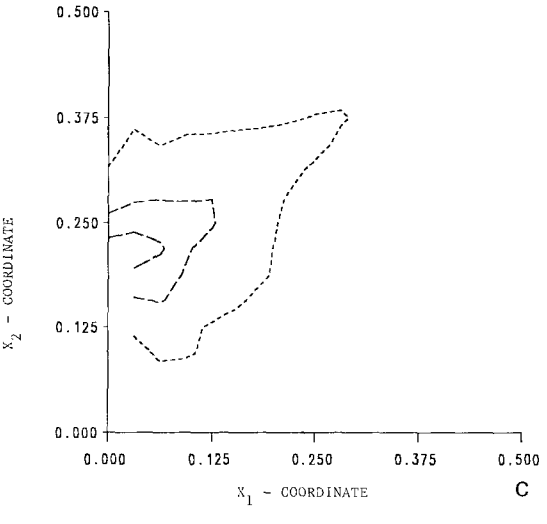
0.500
0.375
0.250
0.125
0.000
0.000
0.125
0.250
0.375
0.500
X_2 - COORDINATE
X_1 - COORDINATE
c

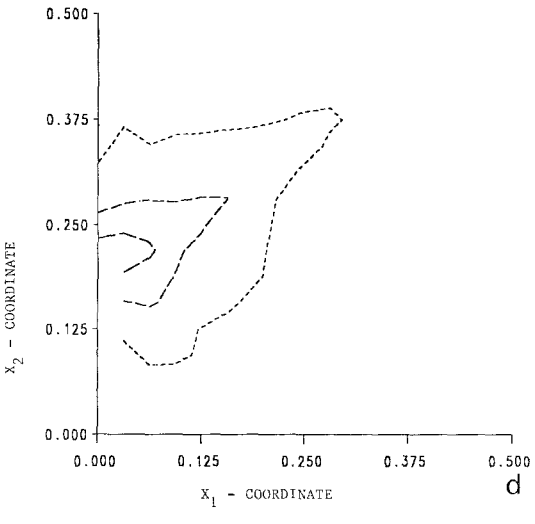
0.500
0.375
0.250
0.125
0.000
0.000
0.125
0.250
0.375
0.500
X_2 - COORDINATE
X_1 - COORDINATE
d

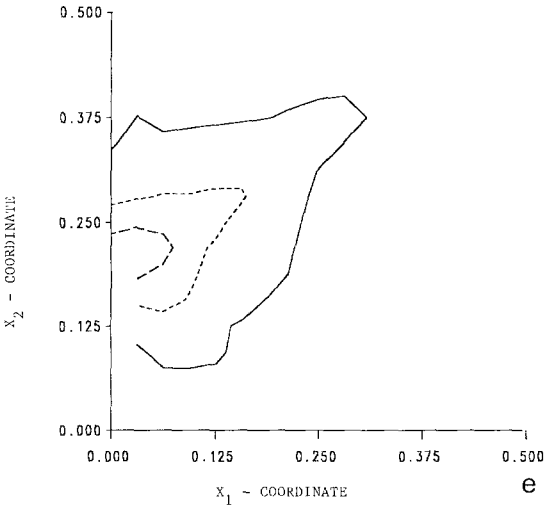
0.500
0.375
0.250
0.125
0.000
0.000
0.125
0.250
0.375
0.500
X_2 - COORDINATE
X_1 - COORDINATE
e

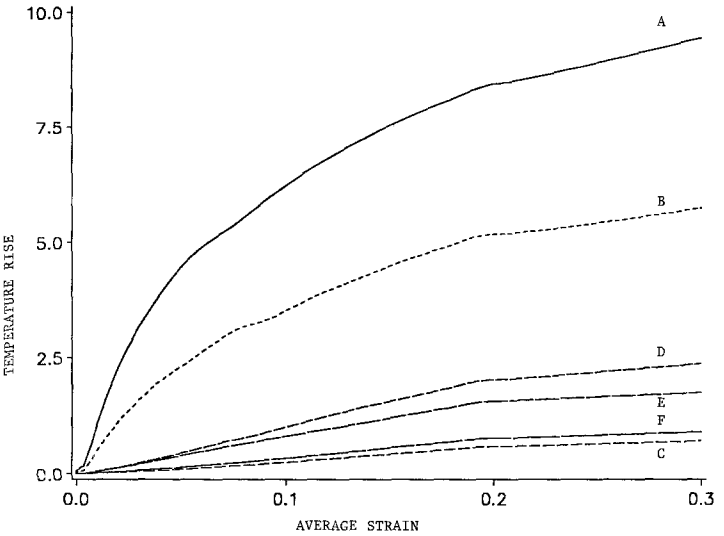

Fig. 4a. Variation of the temperature rise with the average strain at six different points for the horizontally aligned inclusion. Coordinates of these points in the reference configuration are: A (0.2052, 0.000218), B (0.1782, 0.01625), C (0.009525, 0.02621), D (0.4044, 0.00345), E (0.0951, 0.2952), F (0.006907, 0.04353)

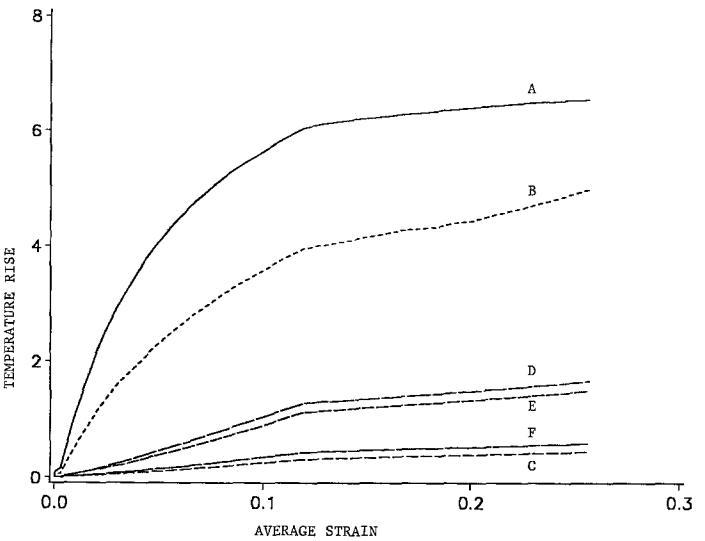

Fig. 4b. Variation of the temperature rise with the average strain at six different points for the vertically aligned inclusion. Coordinates of these points in the reference configuration are: A (0.0002176, 0.20523), B (0.01625, 0.17824), C (0.02621, 0.009525), D (0.00345, 0.4044), E (0.2952, 0.09511), F (0.04353, 0.006907)

Fig. 3. Isotherms plotted in the reference configuration at different values of the average strain with the vertically placed inclusion

(a) $\gamma_{avg} = 0.095$, $\theta_{max} = 6.11$, ---- 2; — — — 4; ——— 6.
(b) $\gamma_{avg} = 0.131$, $\theta_{mag} = 6.85$. See part (a) for values of θ corresponding to different curves.
(c) $\gamma_{avg} = 0.167$, $\theta_{max} = 7.14$. See part (a) for values of θ corresponding to different curves.
(d) $\gamma_{avg} = 0.193$, $\theta_{max} = 7.24$. See part (a) for values of θ corresponding to different curves.
(e) $\gamma_{avg} = 0.248$, $\theta_{max} = 7.74$, ——— 2; ---- 4; — — — 6

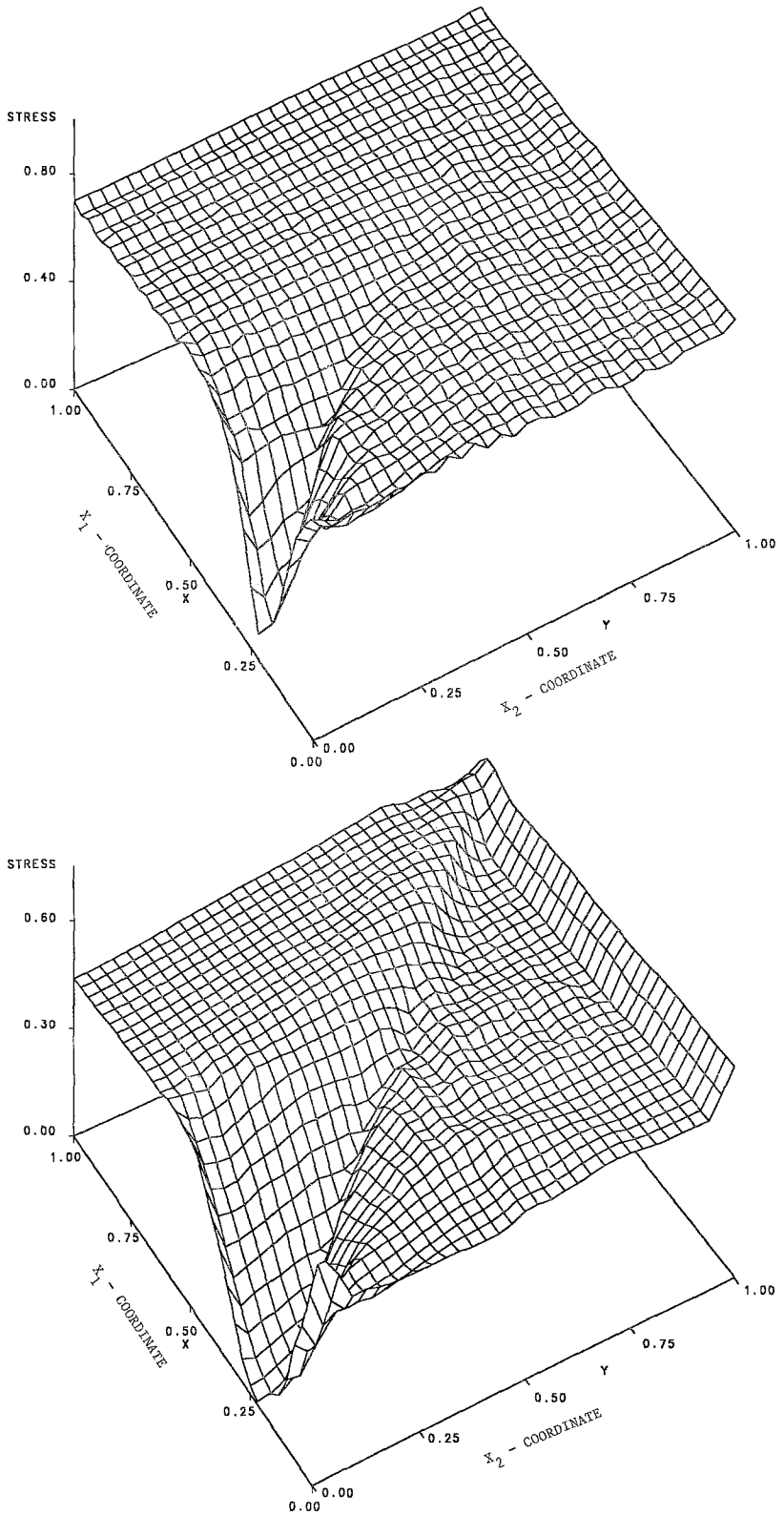

Fig. 5. Distribution of the effective stress within the body at two different values of the average strain with the inclusion aligned along the x_1-axis. (a) $\gamma_{\text{avg}} = 0.0536$, (b) $\gamma_{\text{avg}} = 0.2479$

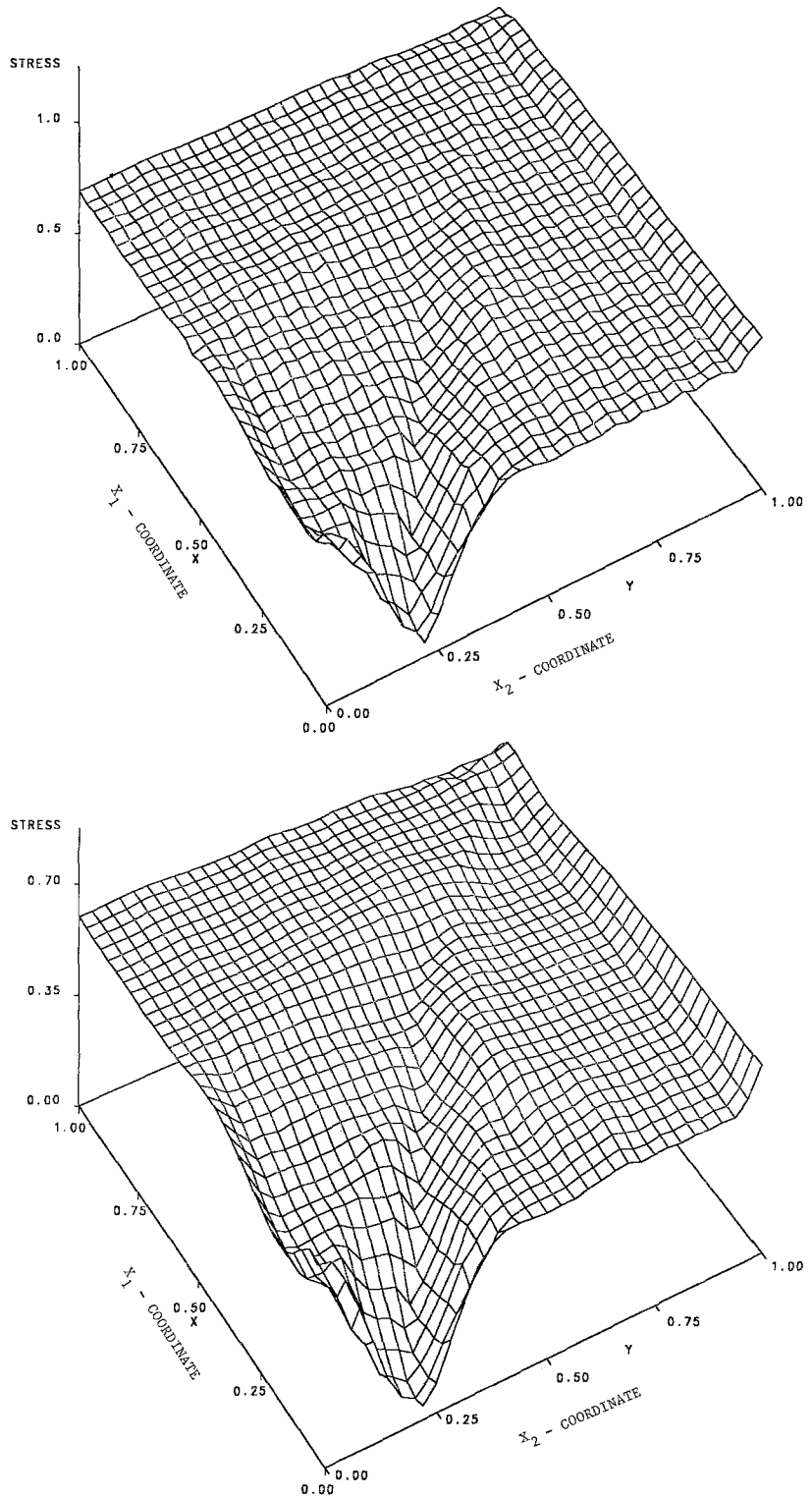

Fig. 6. Distribution of the stress within the body at two different values of the average strain with the inclusion aligned along the x_2-axis (a) $\gamma_{avg} = 0.095$, (b) $\gamma_{avg} = 0.2479$

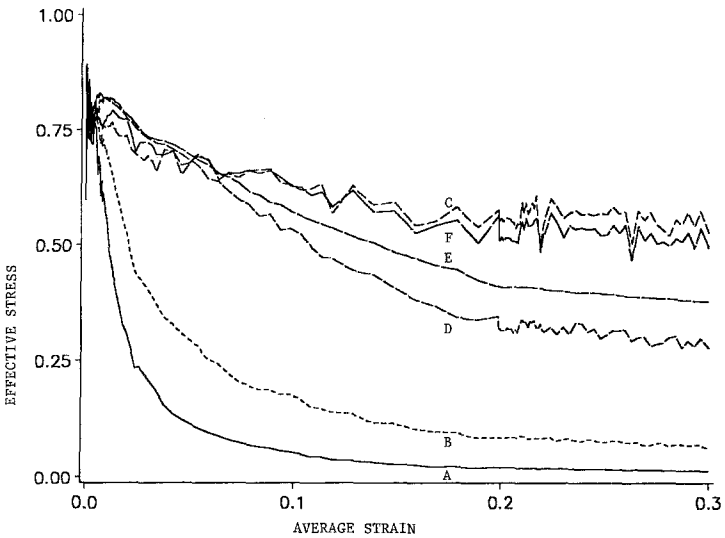

Fig. 7a. Variation of the effective stress with the average strain at six different points for the horizontally aligned inclusion. See Fig. 4a for the coordinates of the six points

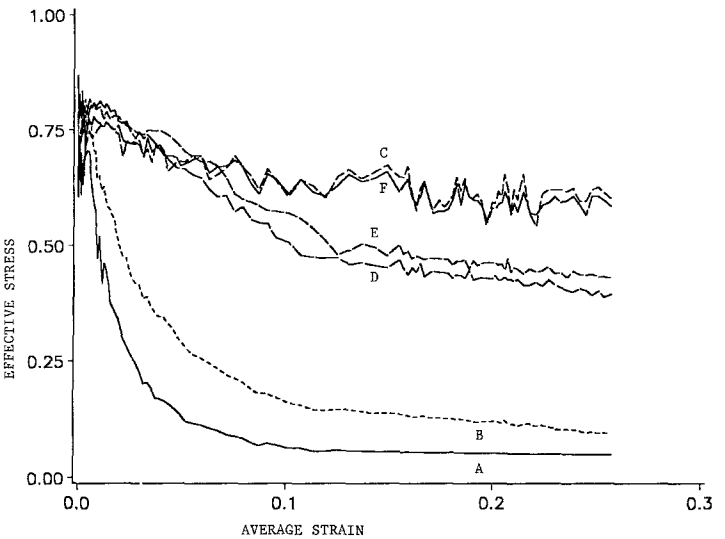

Fig. 7b. Variation of the effective stress with the average strain at six different points for the vertically aligned inclusion. See Fig. 4b for the coordinates of six points

is plotted in Figs. 5a and 5b, and Figs. 6a and 6b for the horizontally and vertically placed inclusions, respectively. In both cases, the stress drops noticeably near the tip of the inclusion and as the band propagates along the 45° direction, the shear stress drops. The rather small drop of the shear stress near the other extremity of the 45° line indicates that the deformation there has not localized as much as it has near the inclusion tip. Batra and Liu [26], [27] used linear thermal softening law with a rather large value of the thermal softening coefficient and found that once the deformation localized near the site of the defect, it propagated quickly along the 45° direction to the other edge. Here the thermal softening is represented by an exponential function and the band propagates slowly leading one to conjecture that the speed of propagation of the shear band is strongly influenced by

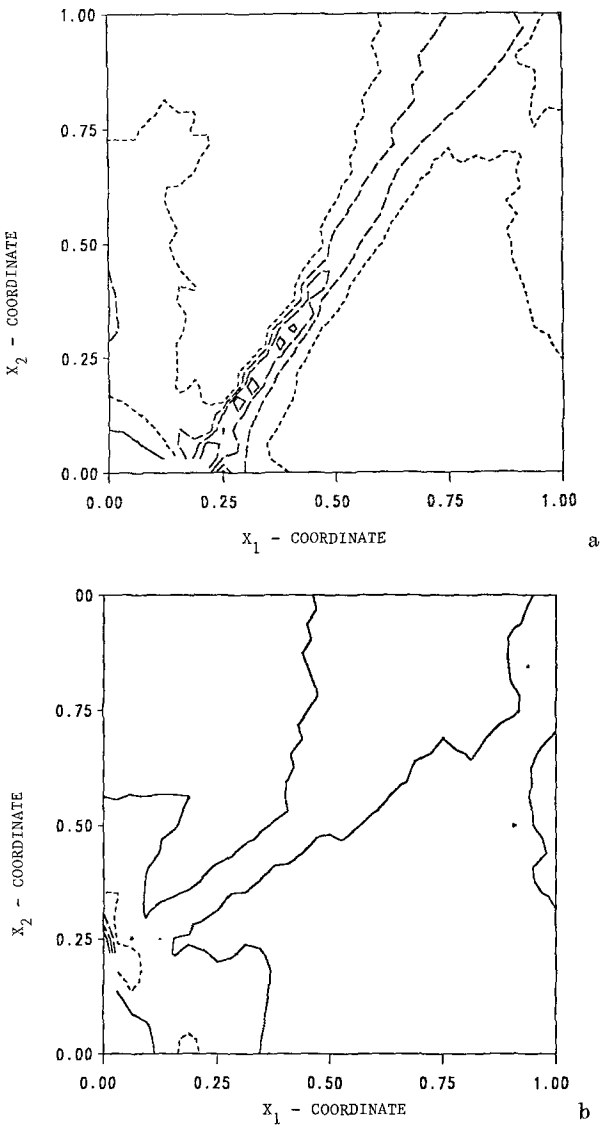

Fig. 8. Contours of the maximum principal logarithmic strain **(a)** horizontally aligned inclusion, $\gamma_{avg} = 0.344$; ——— 0.2, ···· 0.4, — — — — 0.6, ——— ——— 0.8, ——·—— 1.0, **(b)** vertically aligned inclusion, $\gamma_{avg} = 0.248$; ——— 0.3, ···· 0.5, — — — 0.7, ——— ——— 0.9, ——·—— 1.1

the thermal softening law and the value of the thermal softening coefficient used. In Figs. 7a and 7b, we have plotted the variation of the effective stress with the average strain at six points for the horizontally and vertically aligned inclusions. We note that the temperature rise at these points was plotted in Fig. 4. As for the one-dimensional case, the initiation and development of a shear band is accompanied by a rapid drop of the effective stress. The stress drop at the inclusion tip is significantly more than that at the adjoining point considered. At points far removed from the inclusion tip, the stress drops only slightly. The oscillations in the value of the effective stress at points far away from the inclusion tip is possibly due to the fact that the rate of deformation there is small and the stress computations involve the division of one small number by another small number. For each case studied, the effective stress near the inclusion tip reaches a plateau after the rapid drop.

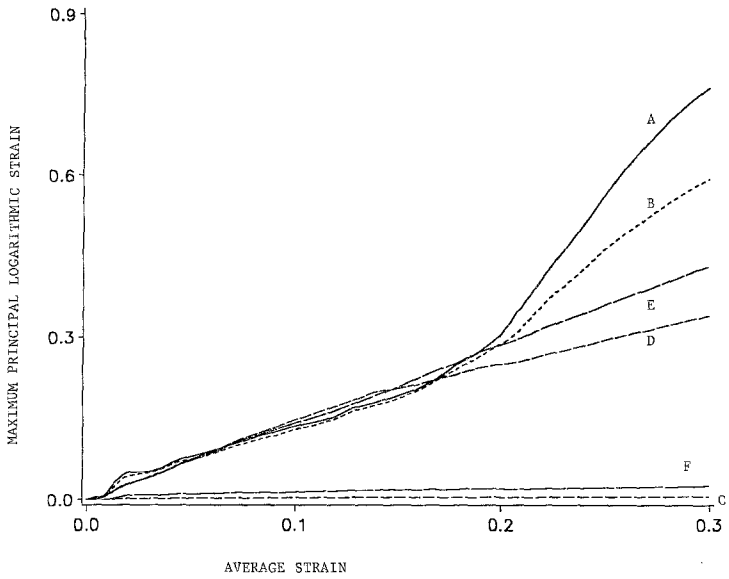

Fig. 9a. Variation of the maximum principal logarithmic strain with the average strain at six different points for the horizontally aligned inclusion. See Fig. 4a for the coordinates of the six points

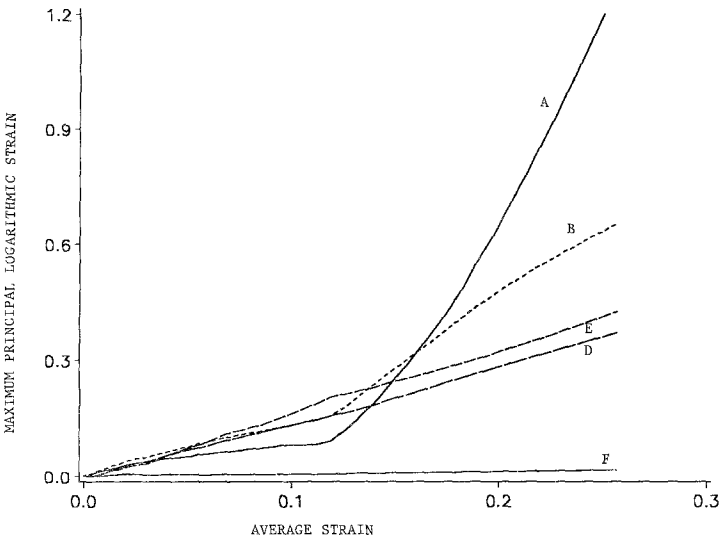

Fig. 9b. Variation of the maximum principal logarithmic strain with the average strain at six different points for the vertically aligned inclusion. See Fig. 4b for the coordinates of the six points

This was not observed in the one-dimensional computations with the linear thermal softening, but was found to be the case [33] when the material behavior was modeled by the Bodner-Partom law.

Figures 8a and 8b depict the contours of the maximum principal logarithmic strain

$$\varepsilon = \ln \lambda_1 \tag{4.3}$$

where λ_1^2 is the maximum eigenvalue of the right Cauchy-Green tensor

$$C_{\alpha\beta} = x_{i,\alpha} x_{i,\beta}. \tag{4.4}$$

Let λ_2^2 and 1 be the other two eigenvalues of $C_{\alpha\beta}$. Since the deformations are nearly isochoric,

$$\ln \lambda_1 \approx -\ln \lambda_2 . \tag{4.5}$$

It is clear from these plots that severe deformations occur in a narrow region. For the horizontally aligned inclusion, the shear band is rather well defined. For the vertically aligned inclusion, contours of higher values of ε have not propagated farther into the deformable block. Note that the nominal strain at which these results are plotted is different in the two cases. However, the variation of ε with the nominal strain at six points plotted in Figs. 9a and 9b reveal that near the inclusion tip ε attains higher values for the vertically aligned inclusion as compared to that for the horizontally aligned elliptic inclusion. For the former case, the curves of ε vs. average strain coincide for points E and F. In each case, ε increases slowly first near the inclusion tip. Subsequently, the rate of growth of ε picks up sharply and the region surrounding the inclusion tip is deformed more intensely as compared to the rest of the body. Note that the values of the nominal strain at which s_e drops sharply and ε increases rapidly at the same point near the inclusion tip are different; the stress drop occurs first. Thus, even though the material in a small neighborhood of the inclusion tip has weakened, the surrounding material contributes significantly to the load carrying capacity of the member and constrains the weaker small region from deforming severely. Thus, if one adopts the view point that a shear band initiates when the maximum logarithmic strain at a point increases sharply, then the initiation of the shear band in this case occurs considerably after the shear stress has dropped precipitously. This differs from the results of the one-dimensional computations [19], [33] in which the precipitous drop of the shear stress and the sharp increase of the plastic strain at a point occur simultaneously.

Figure 10 depicts the velocity field within the deforming material at an average strain of 25% and when the major axis of the inclusion is along the x_1-axis. There is a noticeable change in the velocity field across the 45° line along which a shear band has formed. Johnson [34] has recently pointed out that Tresca [35] and Massey [36] observed shear bands in the form of a cross with sides inclined at $\pm 45°$ to the direction of loading during hot forging of certain metals. They asserted that the tangential velocity is discontinuous across these bands. The velocity field plotted in Fig. 10 supports this to some degree. We add that the velocity field plotted in Fig. 3 of Batra and Liu's paper [26] vividly demonstrates that the tangential velocity suffers a jump across the shear band. The velocity field for the vertically aligned inclusion exhibits a behavior similar to that shown in Fig. 10 and the plots are not included herein.

The average compressive force F_y given by

$$F_y = -\int_0^1 \sigma_{22}\, dx_1 \tag{4.6}$$

versus the nominal strain is plotted for the two cases in Fig. 11. The curve of dash lines represents the case when there is no inclusion present. The integral in Eq. (4.6) is evaluated by using values of σ_{22} at quadrature points on the top loading surface. Initially, the applied force increases almost linearly in each case due to the linear increase of the applied velocity. The presence of the inclusion necessitates initially a larger force as compared to that required to deform the homogeneous block. Due to the heating of the block caused by the ensuing plastic deformation, the material softens and the load required to deform it decreases. This decrease in the load is more for the block with an inclusion because of the

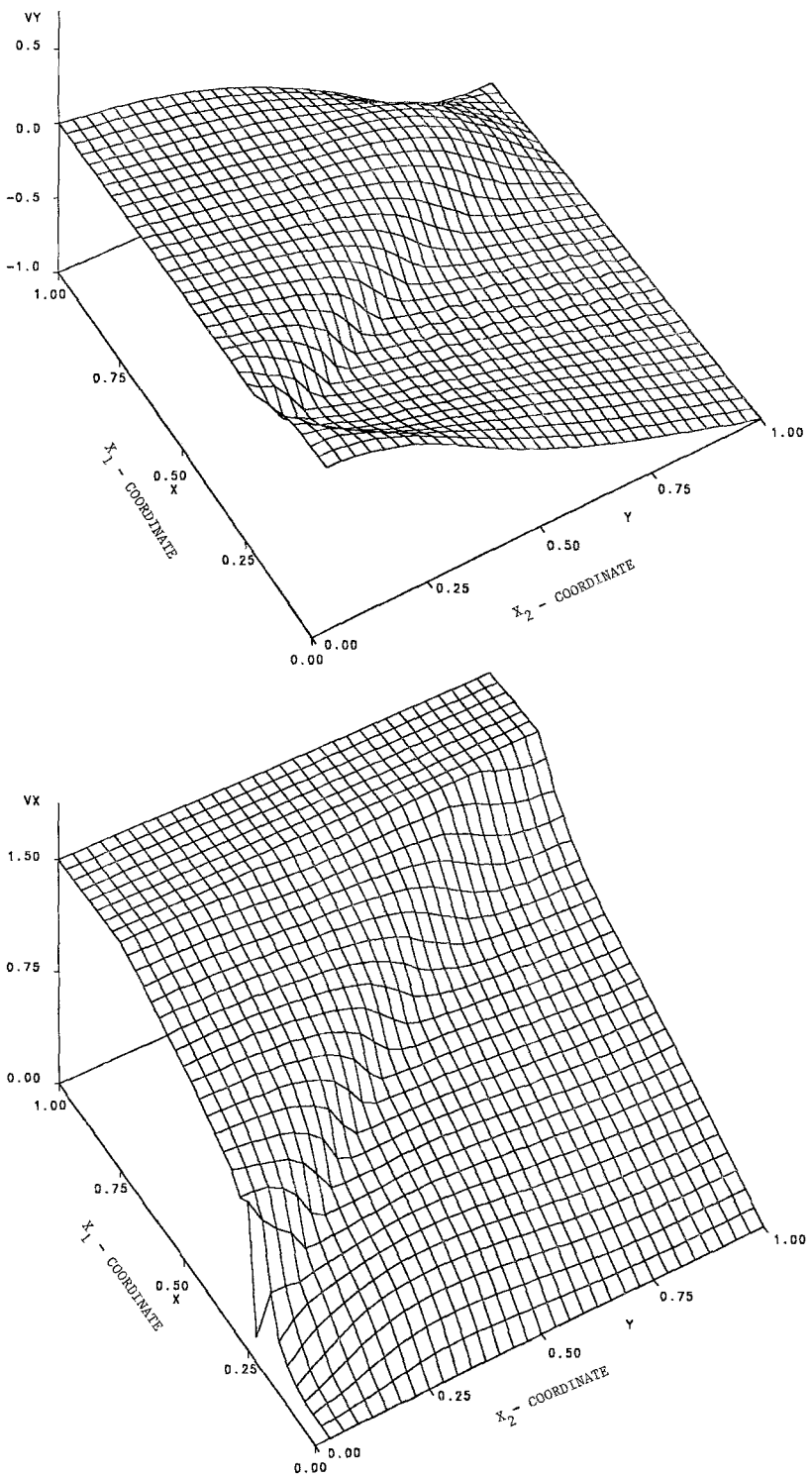

Fig. 10. Velocity distribution within the block for the inclusion along the x_1-axis at an average strain of 0.2478

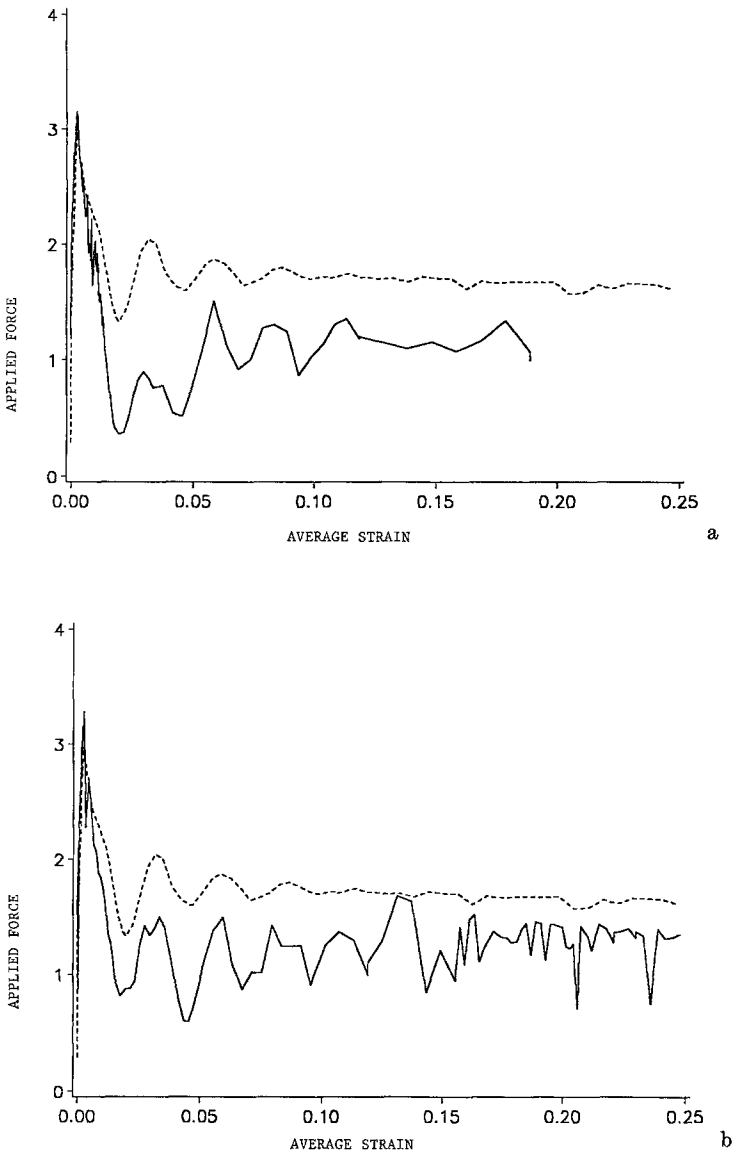

Fig. 11. Load-average strain curves for (a) horizontally aligned inclusion (solid line), (b) vertically aligned inclusion (solid line). The dash line represents the load-displacement curve when there is no inclusion present in the block

nucleation of a shear band near the tip of the inclusion. However, subsequent to the initiation of a shear band, the applied force stays lower than that for the homogeneous block signifying the lower load carrying capacity of the member once a shear band develops in it. The oscillations in the applied force are more for the vertically aligned inclusion. These can be attributed, at least partially, to the fact that the deformation in the top row of elements is not homogeneous and the computations of tractions at the boundary points is less accurate as compared to the solution within the block. Note that contours of different values of ε and θ arrive at some elements in the top row at different instants and thus affect the stress distribution in the elements. We believe that the use of a finer mesh would

decrease the oscillations in F_y, but this could not be verified because of the limited computational resources available to us. Also, a finer mesh would improve the resolution of the deformation within the band.

5 Conclusions

The problem of the initiation and subsequent growth of a shear band in plane strain thermomechanical deformations of a viscoplastic block containing an elliptical inclusion has been studied by the finite element method. It is found that a shear band nucleates at the tip of the inclusion and propagates along the direction of maximum shearing. As the strain rate within the band increases, the effective stress in it drops and the temperature continues to increase. The maximum computed temperature when the effective stress had dropped to nearly zero equalled 937 °C. At a point near the inclusion tip the effective stress drops rapidly first. This is followed, much later, by a sharp increase in the maximum principal logarithmic strain at the same point. This delay is possibly due to the constraining effects of the relatively strong material surrounding the weakened material near the inclusion tip.

Acknowledgements

This work was supported by the U.S. National Science Foundation Grant MSM 8715952 and the U.S. Army Research Office Contracts DAAL 03-88-K-0184 and DAAL 03-89-K-0050 to the University of Missouri-Rolla. Some of the computations were performed on the IBM 3090 vector machine in Columbia, MO under the trial program.

References

[1] Zener, C., Hollomon, J. H.: Effect of strain rate on plastic flow of steel. J. Appl. Phys. **14**, 22–32 (1944).
[2] Recht, R. F.: Catastrophic thermoplastic shear. ASME J. Appl. Mech. **31**, 189–193 (1964).
[3] Staker, M. R.: The relation between adiabatic shear instability strain and material properties. Acta Met. **29**, 683–689 (1981).
[4] Clifton, R. J.: Material response to ultra high loading rates. NRC National Material Advisory Board (U.S.) Report **356** (1980).
[5] Molinari, A., Clifton, R. J.: Analytic characterization of shear localization in thermoviscoplastic materials. J. Appl. Mechs. **54**, 806–812 (1987).
[6] Burns, T. J.: Approximate linear stability analysis of a model of adiabatic shear band formation. Quart. Appl. Math. **43**, 65–83 (1985).
[7] Wright, T. W.: Steady shearing in a viscoplastic solid. J. Mech. Phys. Solids **35**, 269–282 (1987).
[8] Anand, L., Kim, K. H., Shawki, T. G.: Onset of shear localization in viscoplastic solids. Massachusetts Institute of Technology Report, 1986.
[9] Bai, Y. L.: A criterion for thermoplastic shear instability. In: Shock waves and high strain rate phenomenon in metals (Meyers, M. A., Murr, L. E., eds.), pp. 277–283. New York: Plenum Press 1981.
[10] Coleman, B. D., Hodgdon, M. L.: On shear bands in ductile materials. Arch. Rat. Med. Anal. **90**, 219–247 (1985).
[11] Moss, G. L.: Shear strain, strain rate and temperature changes in adiabatic shear band. In: Shock waves and high strain rate phenomenon in metals (Meyer, M. A., Murr, L. E., eds.), pp. 299–312. New York: Plenum Press 1981.
[12] Costin, L. S., Crisman, E. E., Hawley, R. H., Duffy, J.: On the localization of plastic flow in mild steel tubes under dynamic torsional loading. Int. Phys. Conf. Ser. No. **47**, 90–100 (1979).
[13] Marchand, A., Duffy, J.: An experimental study of the formation process of adiabatic shear bands in a structural steel. J. Mechs. Phys. Solids **36**, 251–283 (1988).

[14] Clifton, R. J., Duffy, J., Hartley, K. S., Shawki, T. G.: On critical conditions for shear band formation at high strain rates. Scripta Metallurgica **18**, 443—450 (1984).
[15] Merzer, A. M.: Modeling of adiabatic shear band development from small imperfections. J. Mech. Phys. Solids **30**, 323—338 (1982).
[16] Wu, F. H., Freund, L. B.: Deformation trapping due to thermoplastic instability in one-dimensional wave propagation. J. Mech. Phys. Solids **32**, 119—132 (1984).
[17] Wright, T. W., Batra, R. C.: The initiation and growth of adiabatic shear bands. Int. J. Plasticity **1**, 205—212 (1985).
[18] Wright, T. W., Batra, R. C.: Adiabatic shear bands in simple and dipolar plastic materials. In: Proc. IUTAM Symposium on macro- and micro-mechanics of high velocity deformation and fracture (Kawata, K., Shioiri, J., eds.), pp. 189—201 Berlin—Heidelberg—New York: Springer 1987.
[19] Wright, T. W., Walter, J. W.: On stress collapse in adiabatic shear bands. J. Mech. Phys. Solids **35**, 701—720 (1987).
[20] Batra, R. C.: The initiation and growth of, and the interaction among adiabatic shear bands in simple and dipolar materials. Int. J. Plasticity **3**, 75—89 (1987).
[21] Batra, R. C.: Effect of material parameters on the initiation and growth of adiabatic shear bands. Int. J. Solids and Structures **23**, 1435—1446 (1987).
[22] Batra, R. C.: Effect of nominal strain-rate on the initiation and growth of adiabatic shear bands. J. Appl. Mechs. **55**, 229—230 (1988).
[23] LeMonds, J., Needleman, A.: Finite element analyses of shear localization in rate and temperature dependent solids. Mechs. Materials **5**, 339—361 (1986).
[24] LeMonds, J., Needleman, A.: An analysis of shear band development incorporating heat conduction. Mechs. Materials **5**, 363—373 (1986).
[25] Needleman, A.: Dynamic shear band development in plane strain. J. Appl. Mechs. **56**, 1—8 (1989).
[26] Batra, R. C., Liu, D. S.: Adiabatic shear banding in plane strain problems. J. Appl. Mechs. **56**, 527—534 (1989).
[27] Batra, R. C., Liu, D. S.: Adiabatic shear banding in dynamic plane strain compression of a viscoplastic material. Int. J. Plasticity **6**, 231—246, 1990.
[28] Anand, L., Lush, A. M., Kim, K. H.: Thermal aspects of shear localization in viscoplastic solids. Thermal aspects in manufacturing. In: ASME-PED-Vol. **30**, (ATTIA, M. H., Kops, L., eds.), 89—103 (1988).
[29] Shockey, D. A., Seaman, L., Curran, D. R.: The influence of microstructure features on dynamic fracture. In: Metallurgical effects at high strain rates (Rhode, R. W., Butcher, B. M., Holland, J. R., Karnes, E. H., eds.), p. 473. New York—London: Plenum Press 1973.
[30] Bathe, K. J.: Finite element procedures in engineering analysis. Englewood Cliffs: Prentice-Hall 1982.
[31] Hughes, T. J. R.: The finite element method. Linear static and dynamic finite element analysis. Englewood Cliffs: Prentice Hall 1987.
[32] Batra, R. C., Liu, D. S.: Dynamic shear band development in thermally softening viscoplastic materials. Proc. 2nd Int. Symp. Plasticity and its Current Applications (Khan, Akhtar, S., Tokuda, M., eds.), pp. 435—438. Pergamon Press 1989.
[33] Batra, R. C., Kim, C. H.: Effect of viscoplastic flow rules on the initiation and growth of shear bands at high strain rates. J. Mechs. Phys. Solids (in press).
[34] Johnson, W.: Henri Tresca as the originator of adiabatic heat lines. Int. J. Mech. Sci. **29**, 301—310 (1987).
[35] Tresca, H.: On further application of the flow of solids. Proc. Inst. Mech. Engr. **30**, 301—345 (1878).
[36] Massey, H. F.: The flow of metal during forging. Proc. Manchester Assoc. Engineers, pp. 21—26, 1921. Reprinted by the National Machinery Co., Tiffon, Ohio 1946.

Authors' address: Z. G. Zhu and R. C. Batra, Department of Mechanical and Aerospace Engineering and Engineering Mechanics, University of Missouri-Rolla, Rolla, MO 65401-0249, U.S.A.